Korean J. Chem. Eng., 34(11), 2966-2977 (2017)
DOI: 10.1007/s11814-017-0197-8

pISSN: 0256-1115
eISSN: 1975-7220

Interpretation and diagnosis of fouling progress in membrane bioreactor plants using a periodic pattern recognition method

KiJeon Nam*, MinJeong Kim, Seungchul Lee*, Soonho Hwangbo*, and ChangKyoo Yoo*,†**

*Department of Environmental Science and Engineering, College of Engineering, Kyung Hee University, Seocheon-dong 1, Giheung-gu, Yongin-si, Gyeonggi-do 17104, Korea
**Korea Railroad Research Institute, 76, Cheoldobangmulgwan-ro, Uiwang-si, Gyeonggi-do 16105, Korea
(*Received 17 April 2017 • accepted 13 July 2017*)

Abstract−Fouling is a principal constraint of membrane bioreactors (MBRs). It blocks the wide use of MBRs and aggravates the ability of MBRs. Trans-membrane pressure (TMP) is measured simply from MBRs and is a useful factor for evaluating fouling phenomena such as fouling mechanisms. Fouling mechanism diagnosis based on a measured TMP was used to evaluate MBRs operation conditions. However, diagnosis of MBR conditions is difficult due to the dynamic conditions of MBRs. Therefore, we used differential calculus, exponential weighted moving average (EWMA) and fast Fourier transform (FFT) to determine a periodic pattern for diagnosing fouling mechanisms in the dynamic operating conditions of MBRs. The periodic pattern was reflected in the operating conditions of MBRs, based on the fouling mechanism using TMP. We used two data sets obtained from pilot-scale MBR to suggest a periodic pattern and validated the proposed method using a lab-scale MBR experiment. Consequently, the suggested periodic pattern can diagnose fouling mechanisms using the proposed method, because the methods can be adjusted under the dynamic conditions of MBRs.

Keywords: Membrane Bioreactor (MBR), Fouling Mechanism, Periodic Pattern Recognition, Differential Calculus, Fast Fourier Transform (FFT)

INTRODUCTION

The membrane bioreactor (MBR) process, which combines conventional biological wastewater treatment and physical membrane processes, has been widely used in wastewater treatment. Compared to conventional biological wastewater treatment, which uses a sedimentation and a sludge thickener performed by gravity, the MBR process has short treatment times and its space-saving size [1,2]. Furthermore, it guarantees high quality of effluent, which contains low concentrations of suspended solids, organic matter, and biological nutrients due to the filtering of bacteria and micro pollutants [3].

Despite these advantages, wide application of the MBR process is constrained due to membrane fouling. The attachment of particulate matters onto the membrane's surface or pores is the primary phenomenon causing membrane fouling [4]. It causes a decrease in the permeate flux under constant-pressure operational modes or an increase in the trans-membrane pressure (TMP) under constant-flux operational modes. This results in higher operational costs for membrane aeration and has a harmful effect on the environment due to the use of additional chemicals for membrane cleaning [5]. Fouling can typically be attributed to four types of mechanisms, which are complete blocking, intermediate blocking, cake filtration, and standard blocking according to the particle's sedimentation location, such as the surface or inside of the membrane, and the accumulated layer configuration, such as gel or cake layer [6]. In addition, fouling can be prevented by using the membrane-cleaning method determined by the fouling mechanism. Fouling mechanisms, which lead to external or internal fouling, and a gel or cake layer, are used to determine the membrane cleaning method, such as physical cleaning and chemical cleaning. Physical cleaning, which changes hydrodynamics, temperature, and turbulence, kinetically removes foulant sedimentation from the membrane material. Chemical cleaning modifies a solution's chemistry and influences the foulants accumulated on the membrane surface of the gel layer to decompose into the liquid [7,8]. Therefore, accurate and precise diagnosis of a fouling mechanism is necessary to apply the proper membrane cleaning method and for economical and environmentally friendly MBR operation.

Recently, several studies have focused on the diagnosis of fouling mechanism progress based on an experimental method with statistical monitoring [9] and a modeling way [10]. Nourbakhsh et al. [9] measured the membrane-fouling intensity during the experimental process in different operating conditions. They applied a statistical method to investigate the dominant fouling mechanism. Mondal et al. [10] identified sequential fouling mechanism states, intermediate blocking, transient state of the mechanisms and cake formation, under steady flux membrane filtration using three non-dimensional parameters and flux decline phenomena, respectively. However, these studies were conducted in a steady state, where it is assumed that only two fouling mechanisms are dominant in beginning or overall fouling processes. This assumption was not able to

†To whom correspondence should be addressed.
E-mail: ckyoo@khu.ac.kr

capture the varied fouling mechanisms in an actual MBR process according to operational time.

An actual MBR plant is affected by complex fouling mechanisms, which have various types of foulants and surface characteristics [11,12]. Therefore, a new diagnosis method for fouling mechanism progress that considers the dynamics of membrane fouling needs to be developed. To take into consideration the dynamic state process, several investigating and detecting methods, such as differential calculus, exponential weighted moving average (EWMA) and fast Fourier transform (FFT), were applied. Differential calculus can detect instantaneous rate changes under dynamic processes and help to understand mathematical dynamic system modeling [13]. Moreover, EWMA is the most suitable method among statistical process monitoring methods to detect small process shifts by observing previous observations and weighted current observations [14]. FFT is also widely applied in signal processes and analysis, and is useful for analyzing signal characteristics, monitoring, and diagnostic [15]. Therefore, the development of a diagnostic membrane-fouling mechanism, which considers the dynamic state, was our major goal.

We used differential calculus to investigate the time when the fouling mechanism changed. The trans-membrane pressure (TMP) value measured by distinctions between the pressure of influent and effluent water was used for differential calculus. However, ordinary TMP values do not show increasing tendency well. Therefore, the second derivative of the TMP was used to observe the increasing tendency in this study. To consider the dynamic operational conditions in the MBR process, an inflection point was considered as the fouling mechanism changing time. This point was chosen because the increasing tendencies before and after the inflection point on the TMP graph were very different and were affected differently by each fouling mechanism, such as exponentially increasing or slowly increasing. Then, time intervals were determined between inflection points. From these time intervals, the root-mean-square error (RMSE) was used to identify the most dominant fouling mechanism and characteristic of the change in mechanisms. The RMSE value was used as a model evaluation indicator to determine the predominance of the dominant fouling mechanism, which showed the lowest RMSE value among the four fouling mechanisms [16]. In general, a three-stage fouling increase has been observed in MBR: slow fouling, TMP jump [17], and converged TMP. Therefore, an EWMA control chart was applied to the second derivative of TMP to investigate the fouling stage where the current MBR system belongs. Then, FFT was used to formulate a periodic pattern representing variations of the fouling mechanism. FFT is a method of converting a signal in the time domain to the frequency domain [18].

THEORY

1. Four Fouling Mechanism Model under Constant Flux Filtration

The trans-membrane pressure (TMP) of the difference between feed and permeate pressure is continuously measured in the MBR process. Tendency of the continuously measured TMP has obvious information to diagnose fouling mechanism condition of membrane. Four mechanisms are typically used to explain membrane fouling condition depending on the monitored TMP tendency [5, 17]. (1) Cake filtration: when particles accumulate on the surface of a membrane in a permeable cake. (2) Intermediate blocking: when some of the particles are stopped up pores and the remainders of the particles are accumulated on top of the deposited particles. (3) Complete blocking: when particles stop up a pore entrance. (4) Standard blocking: when particles accumulate on the inside of membrane pores [19]. The blocking filtration equation for four fouling mechanisms under constant flux filtration mode can be expressed as follows:

$$\frac{d^2t}{d(\Delta P)^2} = k\left[\frac{dt}{d(\Delta P)}\right]^n \quad (1)$$

where ΔP is the filtration pressure variation; t is the filtration time; k is the resistance coefficient determined by the MBR operating conditions, such as the filter medium and filtration conditions; and n is the dimensionless blocking index that indicates the fouling mechanism model: n=2 for intermediate blocking, n=5/3 for standard blocking, and n=3/2 for complete blocking. In Eq. (1), $dt/d(\Delta P)$ is proportional to the instantaneous hydraulic permeability, which is the inverse of the instantaneous resistance. The filtration pressure variation of cake filtration is proportional to time, so the second derivative is zero [20,21]. Therefore, cake filtration is not applied to the blocking filtration equation under constant flux and it shows a linear increasing tendency when compared with other fouling mechanisms. On the other hand, complete blocking has the lowest n value, which results in having the lowest hydraulic permeability among the fouling mechanisms under constant flux filtration mode. According to the lowest instantaneous hydraulic permeability, therefore, TMP rapidly increases in the case of the complete blocking mechanism.

2. Differentiation of TMP Signal

The differentiation of signals finds the slope of a tangent or the derivative of a function at a given point. The concept of the second derivative is similar to that of the first derivative; if the second derivative is negative, positive, or zero at a point, then this point can be considered to be a maximum, minimum or inflection point, respectively [22]. The inflection point is a point on a curve when the curvature changes from concave upward to concave downward or vice versa [23]. In this study, we assumed that the inflection point was a fouling mechanism changing time, because the before and after curvature of the inflection point had different increasing tendencies determined by each of the fouling mechanisms.

3. Stages of Fouling Progress

In general, fouling is divided into three stages: conditioning fouling, slow fouling, and TMP jump. The conditioning fouling stage is the initial short-term increase in TMP when an interaction occurs between the membrane surface and soluble microbial products (SMP) or extra-cellular polymeric substances (EPS) [24]. In the present study, the conditioning fouling stage was omitted due to its relatively short term compared to the other stages. After the conditioning fouling stage, most of the membrane surface is continuously covered by EPS and SMP. Therefore, in the slow fouling stage, the increase in TMP can be expressed as linear or weakly exponential [25]. The TMP jump stage, which increases the inoperabil-

ity of the membrane, can be described as exceeding a critical flux when permeation is expedited in less fouled areas of the membrane. Therefore, a measured TMP in the TMP jump stage that sharply increases can be expressed as rapidly exponential [26,27]. After the TMP jump stage, almost the entire membrane surface is fouled with colloidal, biological, and organic types of foulants. This phenomenon prompts the converging of TMP to a certain value. Chang et al. [28] showed the steady converged state of suction pressure after the critical flux, depending on the different imposed fluxes in a lab-scale submerged hollow fiber module. The converged TMP stage can be explained by the low compressibility that occurs due to low protein layer resistance provoking a very slow increase and convergence [29].

4. EWMA Control Chart

The exponentially weighted moving average (EWMA) control chart is a statistic monitoring method used to monitor the process mean and variance. Control charts have been used to monitor production processes and to detect abnormal operating conditions. Among the several control charts, the EWMA control chart is an effective monitoring method for detecting small to moderate shifts in the mean of the process [30].

One of the three lines involved in the EMWA control chart is the mean of the measured values called a centerline (CL). An upper control limit (UCL) is placed at a value three-times above the standard deviation of CL. A lower control limit (LCL) is placed at a value three-times below the standard deviation of CL. When the measured value exceeds the UCL or LCL, then the process has an abnormal condition or changed condition at that time. The equation for calculation of EWMA is as follows [31]:

$$Z_i=\lambda X_i+(1-\lambda)Z_{i-1} \tag{2}$$

$$\begin{aligned} &LCL=\mu_0-3\sigma\sqrt{\frac{\lambda}{2-\lambda}(1-(1-\lambda)^{2i})},\ CL=\mu_0,\\ &UCL=\mu_0+3\sigma\sqrt{\frac{\lambda}{2-\lambda}(1-(1-\lambda)^{2i})} \end{aligned} \tag{3}$$

where Z_i is the EWMA of the measured data at time i, X_i is the current information, Z_{i-1} is the past information, μ_0 is the mean of the measured value, σ is the standard deviation of the measured value, and λ is a constant value between 0 and 1. When close to 1, λ weights recent data more heavily and weights older data less heavily. Therefore, the value of λ is generally decided to be approximately 0.25 [32]. In the present study, we used the value of λ=0.25.

5. Fast Fourier Transform (FFT)

Discrete Fourier transform (DFT) is widely used to represent signals of finite length of the Fourier series. DFT can convert discrete signals of the time domain to the frequency domain of the discrete spectrum. FFT is an improved method for computing DFT by using reduced arithmetic operations. FFT has an advantage, in that it reduces the redundancies of complex multiplication by using $N/\log_2 N$ to compare to DFT. FFT can be expressed by the following equation [18,33]:

$$X[k]=\sum_{n=0}^{N-1}x[n]W_N^{nK} \tag{4}$$

where W_N^{nK} is $e^{-2\pi jnk/N}$, $\{x[n]\}_{n=0}^{N-1}$ is a signal, k is the frequency domain ordinal, n is the time-domain ordinal, and N is the length of the sequence.

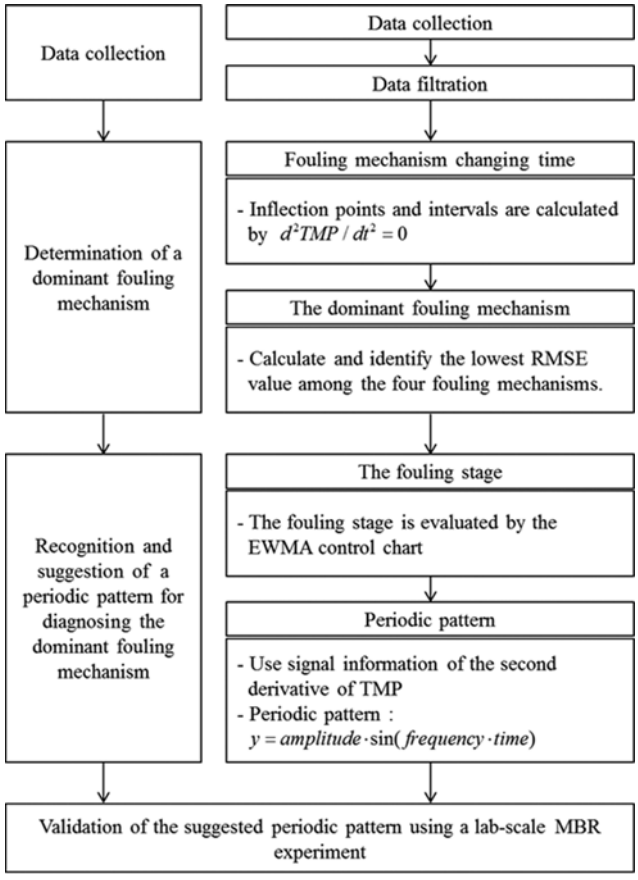

Fig. 1. The proposed scheme for diagnosing the dominant fouling mechanism in the MBR process.

MATERIALS AND METHODS

1. Proposed Method

The proposed method for diagnosing the dominant fouling mechanism, shown in Fig. 1, is broadly divided into three parts: (1) data collection, (2) determination of the dominant fouling mechanism, and (3) suggestion of the periodic pattern. In this study, we carried out this method with three datasets, of which the first two datasets were obtained from a pilot scale MBR process and the last data set was obtained from a lab-scale MBR experiment. To remove abnormal outliers from the datasets, data filtration was conducted using median absolute deviation (MAD). MAD is an easy and robust method for detecting outlier values in univariate statistics [34]. For determining the dominant fouling mechanism, inflection points and intervals were computed using the second derivative of TMP. The most dominant fouling mechanism, which showed the lowest RMSE value, was determined for each inflection point. Then the fouling stage was evaluated using the EMWA control chart. Based on each fouling stage, the periodic pattern for diagnosing the dominant fouling mechanism was suggested. Finally, a lab-scale MBR experiment was used to apply and validate the suggested periodic pattern.

1-1. Determination of the Dominant Fouling Mechanism

The purpose of the second part was to determine the dominant fouling mechanism according to the time intervals of mechanism changing. The second part was divided into two subparts: (1) to calculate the fouling mechanism as it changes in time using differential calculus, and (2) to find the dominant fouling mechanism using RMSE.

The first derivative indicates the variation in the TMP value. Furthermore, the rate of TMP variation can be obtained as the second derivative. If the second derivative of the TMP value was positive or negative at a certain time, then the rate of TMP variation was either at a maximum (i.e., rapidly increasing) or minimum (i.e., slowly increasing), respectively. By calculating the inflection point, the time when the TMP variation rate changed depending on the fouling mechanism variations could be obtained. Here, the time interval of the fouling mechanism variations was decided according to the inflection point time (i.e., first interval: starting point of process ~ first inflection point; second interval: first inflection point ~ second inflection point).

To diagnose the most dominant fouling mechanism at each time interval, four fouling mechanism models (shown in Table 1) were fitted with the TMP values in each time interval. Then, the RSME, which evaluates differences between the observed and modeled values, was used to identify the most suitable fouling mechanism for each time interval among the four mechanisms [19]:

$$\mathrm{RMSE}=\sqrt{\frac{\Sigma_{i=1}^{n}\left[\left(\frac{P}{P_0}\right)_{i.ovserved}-\left(\frac{P}{P_0}\right)_{i.modeled}\right]^2}{n-1}} \tag{5}$$

For instance, for the first time interval, if the intermediate blocking mechanism had the smallest RMSE, then the most dominant mechanism could be diagnosed as intermediate blocking.

1-2. Evaluation of Fouling Stages

In the third part, the periodic pattern for diagnosing the most dominant fouling mechanism was suggested as an expression of trigonometric function. The third part involved the following steps: (1) determining the time where the fouling stage changes (namely, changing time of the fouling stage) using the EWMA, and (2) suggesting the periodic pattern for diagnosing the dominant fouling mechanism in each fouling stage using the FFT.

To determine the changing time of the fouling stage, an EWMA control chart was used to detect small or abnormal shifts in monitoring the process by giving a high weight value to a recently measured value [35]. It is difficult to observe fouling stage variation in raw TMP data. Therefore, the value of the second derivative of TMP, which indicates an increasing variation, such as a linear or exponential increasing tendency, and constant state was used. In the present study, two standard rules of the EWMA control chart were used to detect the TMP rising tendency and fouling stages: (1) if one or more observation was located outside of the control limit and (2) if six observations were placed in succession with an increasing or decreasing trend, these were regarded as signs of the fouling tendency variations [36]. These standard rules enhance the sensitivity of control charts to a small process shift [37].

1-3. Recognition of a Periodic Pattern for Diagnosing the Dominant Fouling Mechanism

The objective of this step was to recognize and suggest a periodic pattern, which is a trigonometric function, such as the sine function, to diagnosis the dominant fouling mechanism at each of the fouling stages determined in the previous step. The second derivative of TMP showed a certain periodic pattern according to time in each of the fouling stages. The FFT can convert this time domain periodic pattern to the frequency domain. Therefore, FFT was used to calculate signal information in order to propose a periodic diagnosis pattern of the fouling mechanism.

Prior to the determination of the periodic pattern for diagnosing the dominant fouling mechanism, a proper signal filter should be applied to eliminate noises, which contain unnecessary information. The second derivative of TMP (shown in '3.1.1. Determination of dominant fouling mechanism') has a high frequency noise, which interrupts application of the FFT method. High frequency noise reduction and reconstruction can improve the quality of the signal of FFT [38,39]. Therefore, a proper filter is necessary to eliminate the high frequency noises and to achieve the proper low frequency signals in FFT from the second derivative of TMP. In this study, a finite impulse response (FIR) filter and low-pass response were used to damp the high frequency noise effect. Digital filters are generally classified into two types: Finite impulse response (FIR) filter and infinite impulse response (IIR) filter. The FIR filter has a stability that is not influenced by distortion and has a linear phase response that is easier to control than the IIR. Therefore, the FIR filter is used in a wider application range than the IIR filter [33]. Furthermore, the low-pass filter can eliminate the high frequency noise, which has a higher frequency value than the specific frequency determined by the user. Therefore, stable periodic signal information is obtained from FFT using the FIR filter and the low-pass filter.

After applying the proper signal filter, the amplitude and frequency of the second derivative of TMP are determined from FFT. Using the results of the FFT, the periodic pattern for diagnosing the dominant fouling mechanism based on sin function can be computed as follows:

$$y=\text{amplitude}\cdot\sin(\text{frequency}\cdot\text{time}) \tag{6}$$

where y is a predicted second derivative of TMP, and amplitude

Table 1. Four mechanistic models of membrane fouling in the MBR process [6]

Model	Equation	Fitted parameter
Cake filtration	$\frac{P}{P_0}=1+K_C J_0^2 t$	K_c [s/m^2]
Intermediate blocking	$\frac{P}{P_0}=\exp(K_i J_0 t)$	K_i [m^{-1}]
Complete blocking	$\frac{P}{P_0}=\frac{1}{1-K_b t}$	K_b [s^{-1}]
Standard blocking	$\frac{P}{P_0}=\left(1-\frac{K_s J_0 t}{2}\right)^{-2}$	K_s [m^{-1}]

P is the TMP value, P_0 is the initial TMP value, J_0 is the initial flux value, t is the MBR process operation time, and K_c, K_i, K_b and K_s are the fitted parameters of each mechanism model

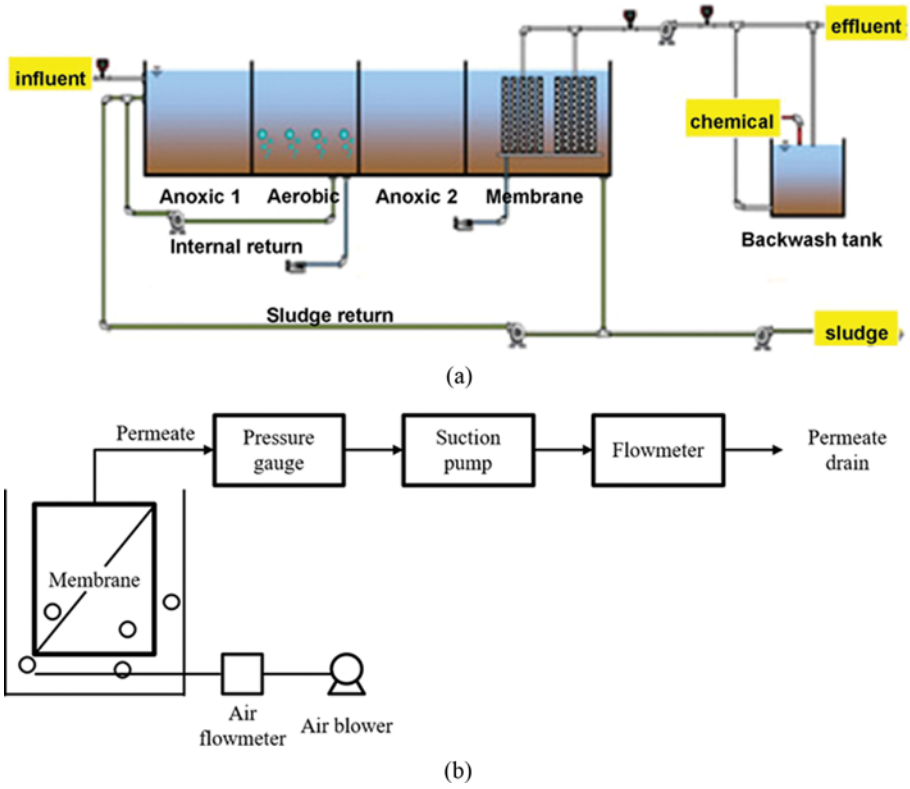

Fig. 2. Configuration of the target MBR process: (a) Pilot-scale MBR plant in Y-city, Korea for proposing the periodic pattern of the fouling mechanism diagnosis [19] and (b) Lab-scale MBR experiment for validating the suggested periodic pattern [40].

and frequency are values obtained from FFT.

2. Pilot Scale MBR and Lab Scale MBR Processes

The processes considered in this study were the pilot-scale MBR plant in Y-city, Korea, and the lab-scale MBR process. The pilot-scale MBR plant data was used to develop a dominant fouling mechanism diagnosis method using a periodic pattern, and the lab-scale MBR process data was used for validation of the study methodology. The configuration of the pilot-scale MBR plant was anoxic1, aerobic, anoxic 2, and membrane reactors, as shown in Fig. 2(a). Table 2 shows the average influent conditions and standard deviation of the pilot-scale MBR plant including flowrate, biological oxygen demand (BOD), chemical oxygen demand (COD), total nitrate (TN), and total phosphorus (TP). The membrane reactor was operated under the constant-flux (or constant-flowrate) mode with a filtration cycle of 10 minutes, of which 9 minutes were for suction and 1 minute was for back-flushing. The sludge retention time (SRT) was more than nine days and the concentration of mixed liquor suspended solid (MLSS) in the membrane reactor was maintained at 7,000-9,000 mg/L. To eliminate foulants on the membrane surface, periodic coarse bubble and back-washing were applied to the membrane.

Table 2. The influent compositions in the pilot-scale MBR plant in Y-city, Korea

Components	Concentration	Standard deviation	Unit
BOD	166	50.37	mg/L
COD	301	74.63	mg/L
T-N	38	10.18	mg/L
T-P	6.4	10.18	mg/L

The configuration of the lab-scale MBR experiment shown in Fig. 2(b) is a bioreactor, pressure gauge, suction pump, and flow

Table 3. The operating conditions in the lab-scale MBR experiment [40]

	Operating factors	Property
Operating conditions	Reactor volume	30 L
	MLSS concentration	10,000-11,000 mg/L
	Number of membrane module	4 modules/reactor
	Membrane operation	Continuous filtration
	Membrane back-washing	No back-washing
	Coarse air flowrate	8 L/min/module (continuous aeration)

meter. Table 3 shows the conditions of the lab-scale MBR experiment. The experiment only focused on physical membrane fouling and, therefore, hydraulic retention time (HRT) and sludge retention time (SRT) were not treated in the experiment. MLSS concentrations of the lab-scale MBR reactor were maintained at around 10,000-11,000 mg/L in a bioreactor, where the amount of attached foulants on the membrane surface depends on the MLSS concentration. The concentrated activated sludge by a centrifugal separator is additionally supplemented, when the MLSS concentration is less than 10,000 mg/L in a bioreactor. Flux was continuously measured to maintain constant-flux mode for observing TMP variation. Physical membrane cleanings, such as in-situ coarse bubble aeration and ex-situ sponge ball cleaning, were conducted to eliminate foulants on the membrane surface [40].

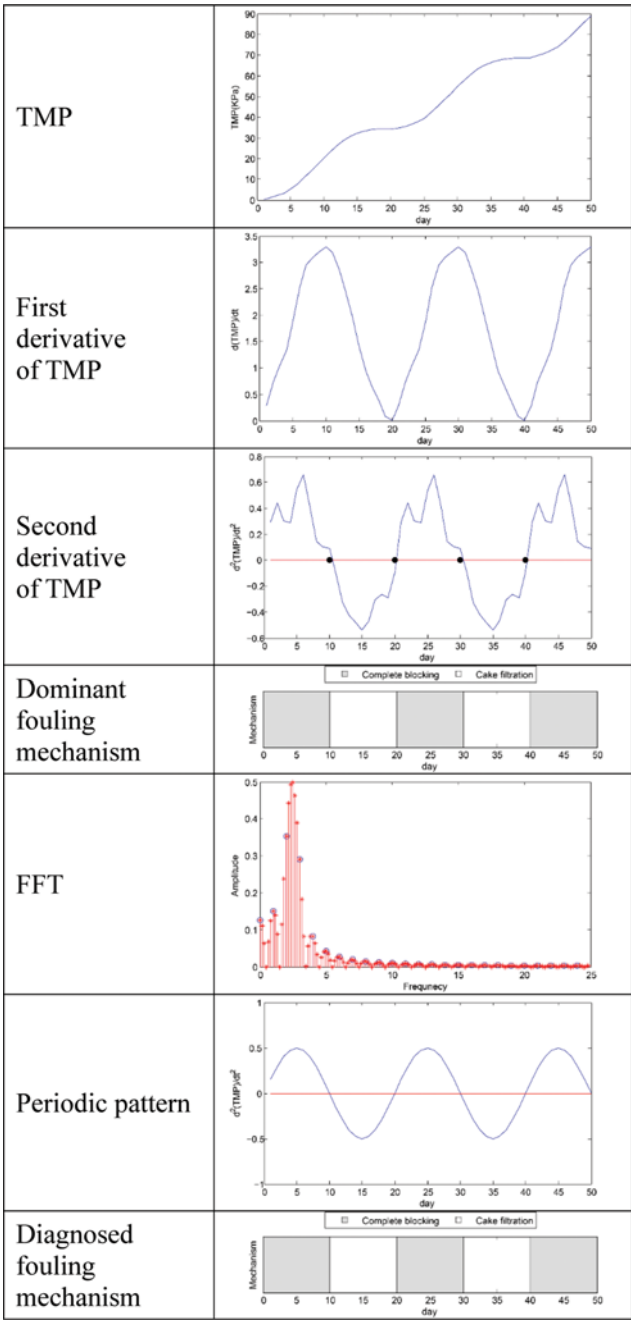

Fig. 3. Detailed steps for diagnosing the dominant fouling mechanism.

3. Procedures of Diagnosis for the Dominant Fouling Mechanism

Detailed steps for diagnosing the dominant fouling mechanism are shown in Fig. 3. The inflection points (drawn as black dots in Fig. 3), indicating the point where the dominant fouling mechanism varied and the intervals of the dominant fouling mechanism changed, were determined by applying the second derivative of TMP. The most dominant mechanism corresponding to each inflection point was computed using RMSE and the tendency of the second derivative (e.g., concave upward or downward) depending on the dominant mechanism was investigated. From the second derivative of TMP, a periodic tendency with 0.5 amplitude and 2 frequency was observed. Once the FFT was applied to the TMP dataset, FFT results of amplitude and frequency identical to those from the second derivative of TMP were obtained. Then, based on the amplitude and frequency values achieved from the FFT, the periodic pattern for identifying the dominant fouling mechanism could be formulated as a sine wave. Therefore, the prediction and diagnosis of the dominant membrane fouling mechanism could be conducted using the periodic pattern with a concave upward and downward tendencies.

RESULTS AND DISCUSSION

1. Determination of the Dominant Fouling Mechanism

Figs. 4(a) and 4(b) show the raw TMP of the pilot-scale MBR process. Moreover, Figs. 4(c) and 4(d) show the first derivative of TMP, which indicates the TMP variation. However, the raw TMP and the first derivative of TMP could not show the dominant fouling mechanism variation effectively. Therefore, the second-order derivate was used to evaluate the time when the TMP variation rate changed depending on the fouling mechanism variation. Figs. 4(e) and 4(f) show the calculated inflection points of each period using the second derivative of TMP for the entire operation time. According to the achieved inflection point, the time intervals when the respective dominant fouling mechanism varied were determined. In period1, five inflection points and six time intervals were determined. In the case of period2, six inflection points and seven time intervals were determined. The higher number of inflection points and time intervals in period2 indicated that the fouling mechanism changes occurred more frequently than during period1. Table 4 shows the RMSE values of each fouling mechanism according to the mechanism changing time intervals by the inflection points. Since the RMSE measures the gap between the model and its observed values, the fouling mechanism with the minimum RMSE was considered to be dominant at each interval when compared to other mechanisms. The results of the most dominant fouling mechanism at each interval are shown in Table 4. Repetitive changes of the cake filtration mechanism and the complete blocking mechanism were mutually observed in period1 and period2 according to the mechanism changing time intervals.

To identify the tendencies of the second derivative of TMP for diagnosing the dominant fouling mechanism changes, the com-

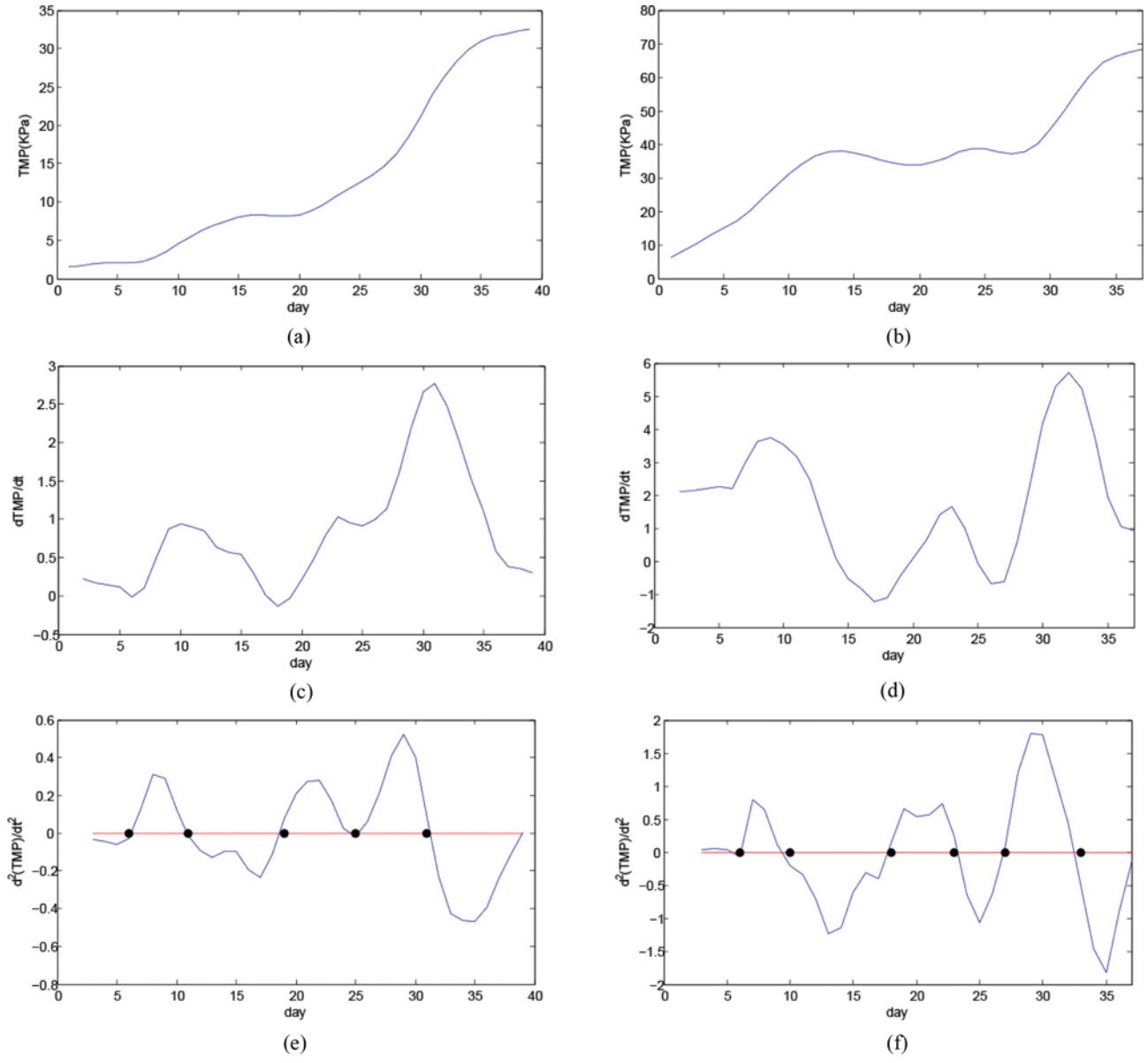

Fig. 4. The raw TMP of the pilot-scale MBR process: (a) period1 and (b) period2; the first derivative of TMP for (c) period1 and (d) period2; and the second derivative of TMP showing the inflection points for (e) peirod1 and (f) period2.

mon characteristics of the second derivative of TMP were investigated. In Fig. 5(a), when cake filtration was the dominant fouling mechanism, then the second derivative of the TMP graph had a concave downward tendency. On the other hand, when complete blocking was the dominant fouling mechanism, the second derivative of the TMP graph revealed a concave upward tendency. Therefore, the second derivative of TMP could indicate the fouling mechanism changing intervals and the variations in the dominant fouling mechanisms. This phenomenon can be explained by Eq. (1), which shows the characteristics of fouling mechanisms. From Eq. (1), complete blocking, which is expressed by the lowest value, can represent the rapid increasing TMP tendency. On the other hand, cake filtration, which has a linear increasing tendency, can represent the linear or gradually increasing TMP tendency. Therefore, the relatively rapid TMP increase of complete blocking signifies the concave upward tendency of the TMP curvature, while the relatively linear or gradually increasing TMP tendency of cake filtration signifies the concave downward tendency of the TMP curvature.

2. Evaluation of the TMP Stage Using the EWMA Control Chart

In Fig. 5, the EWMA control chart of the second derivative of TMP is shown. In period1, points rapidly increased after 25 days, and then they eventually exceeded the upper control limit at 30 days. The linear increasing tendency was changed to a rapidly increasing tendency, which is abnormal in terms of linear increasing. Therefore, this result implies that the variation of TMP increasing occurred at 25 days and the TMP stage changed from slow fouling, which can be expressed by linear TMP increasing, to TMP jump, which can be expressed by a rapid TMP increase in 25 days.

Table 4. Comparison of the RMSE values of the four mechanistic fouling models and the dominant fouling mechanism at each mechanism changing time interval

	RMSE value	#1	#2	#3	#4	#5	#6	#7
Period 1	Day / Mech.	1-6	7-11	12-19	20-25	26-31	32-39	
	Cake filtration	**0.0722**	0.4029	**0.6021**	0.5787	0.9674	**1.5581**	
	Intermediate blocking	0.0853	0.2654	0.7932	0.4968	0.5388	1.9255	
	Complete blocking	0.1026	**0.2049**	1.1977	**0.4353**	**0.1503**	2.4965	
	Standard blocking	0.0933	0.2211	0.9500	0.4639	0.3171	2.1744	
	Dominant mechanism	Cake filtration	Complete blocking	Cake filtration	Complete blocking	Complete blocking	Cake filtration	
Period 2	Day / Mech.	1-6	7-10	11-18	19-23	24-27	28-33	34-39
	Cake filtration	**0.0400**	0.1959	**2.0211**	0.6995	**0.8224**	1.8240	**0.9369**
	Intermediate blocking	0.5460	0.2481	2.0292	0.6837	0.8238	1.2892	1.0186
	Complete blocking	1.7100	**0.1104**	2.0428	**0.6695**	0.8255	**0.9273**	1.1103
	Standard blocking	0.9787	0.1959	2.0353	0.6764	0.8246	1.0782	1.0630
	Dominant mechanism	Cake filtration	Complete blocking	Cake filtration	Complete blocking	Cake filtration	Complete blocking	Cake filtration

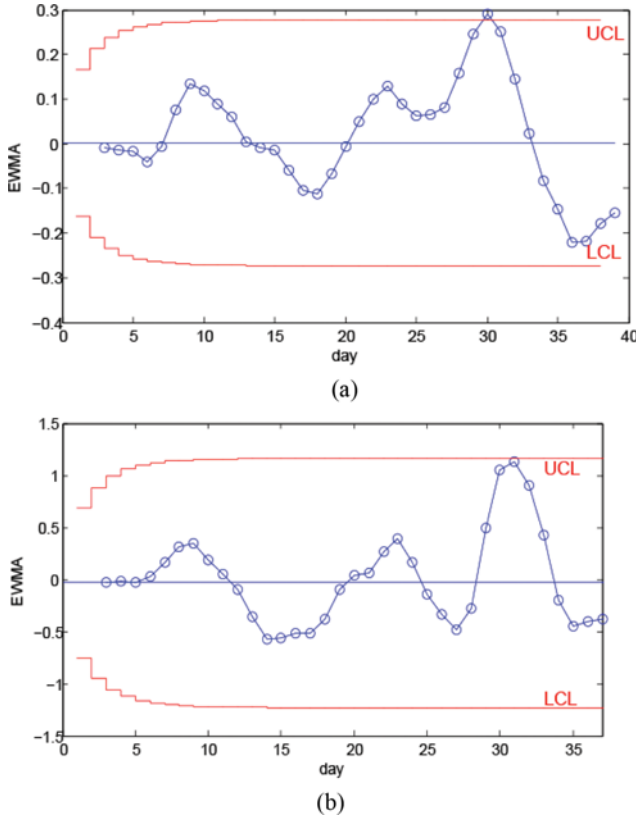

Fig. 5. EWMA control chart of the second derivative of TMP: (a) period1 and (b) period2.

In period2, the points also rapidly increased after 25 days, and then exceeded the ULC at 30 days. This result indicates that the stage of slow fouling changed to TMP jump in period2 after 25 days.

The determined TMP stages corresponded well with the observed raw TMP shown in Figs. 4(a) and 4(b). In period1, the TMP jump stage occurred after 25 days according to the EWMA control chart. The observed TMP increased by 0.40 kPa per day in the slow fouling stage. On the other hand, the TMP increased by 1.67 kPa per day in the TMP jump stage. In period2, the observed TMP increased by 1.60 kPa per day in the slow fouling stage, while the TMP increased by 4.67 kPa per day in the TMP jump stage. These results demonstrate that the TMP stages evaluated using the EWMA control chart were consistent with the observed TMP increasing tendency and verified that the TMP variation in the TMP jump stage was larger than that in the slow fouling stage.

3. Diagnosis of the Dominant Fouling Mechanism by its Periodic Pattern

The raw second derivative of TMP had high frequency noises, which were difficult to graph. Therefore, proper filters were applied to eliminate the high frequency noises. After the proper filters, which were the FIR filter and the low-pass response, were applied, the frequency and amplitude values shown in Figs. 6(a) and 6(b) were obtained. Using the frequency and amplitude values, the respective periodic pattern for diagnosing the dominant fouling mechanism at the slow fouling and TMP stages could be obtained using Eq. (5). In the slow fouling stage in period1, the periodic pattern could be expressed by $y=0.42\cdot\sin(T)$. In the TMP jump stage in period1, the periodic pattern could be expressed by $y=0.21\cdot\sin(2\cdot T)$. Suggested periodic patterns are plotted in Figs. 6(c) and 6(d) with the raw second derivative of TMP. In addition, the results for the filtered FFT and periodic pattern of period2 shown in Fig. 7 are the same as those in Fig. 6. The periodic pattern of the slow fouling in period2 was calculated by $y=0.72\cdot\sin(2\cdot T)$. The periodic pattern of the TMP jump was expressed by $y=1.16\cdot\sin(T)$.

Finally, Fig. 8 shows the summarized results of the proposed method and the periodic pattern for formulating the dominant mechanism at period1 and period2. When compared to the dominant mechanism obtained from the second derivative of TMP, the

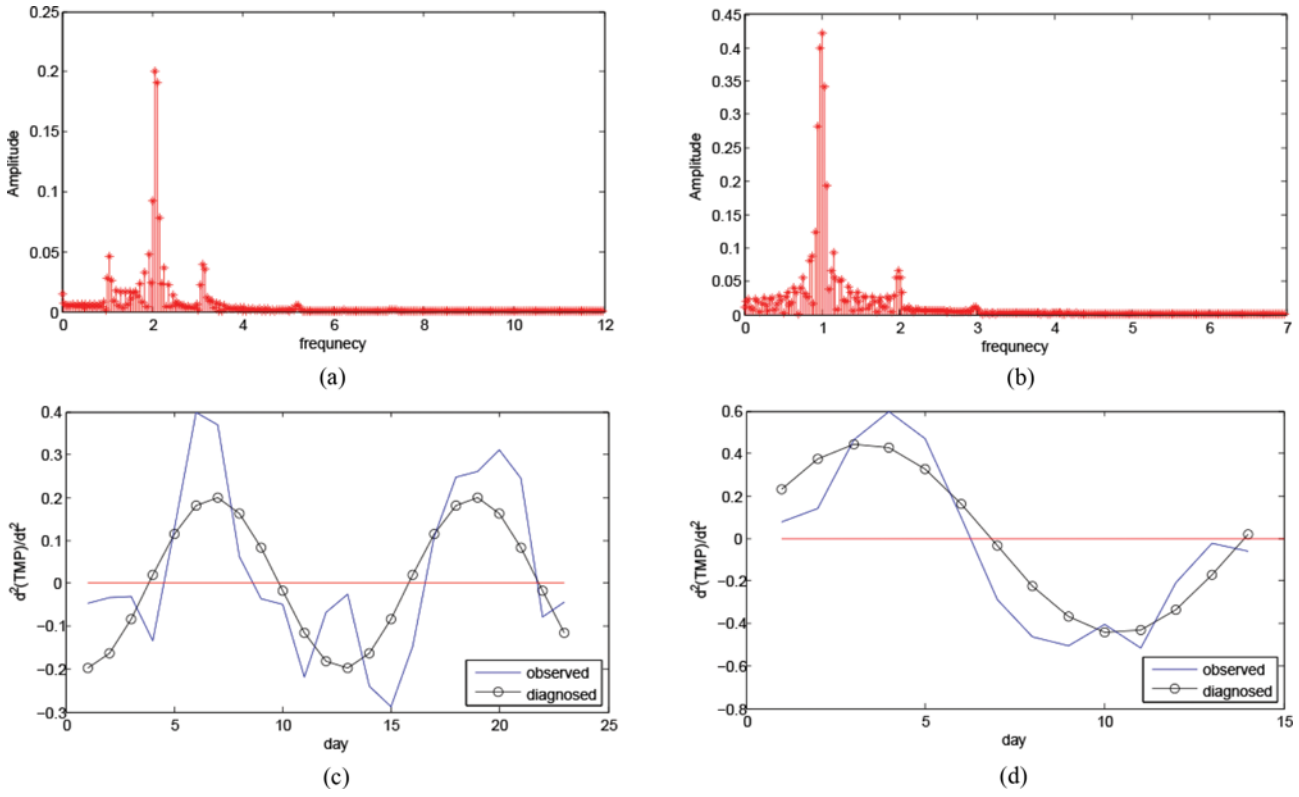

Fig. 6. Period1 results of the FFT for (a) slow fouling and (b) TMP jump, and the periodic pattern using the second derivative of TMP for (c) slow fouling and (d) TMP jump.

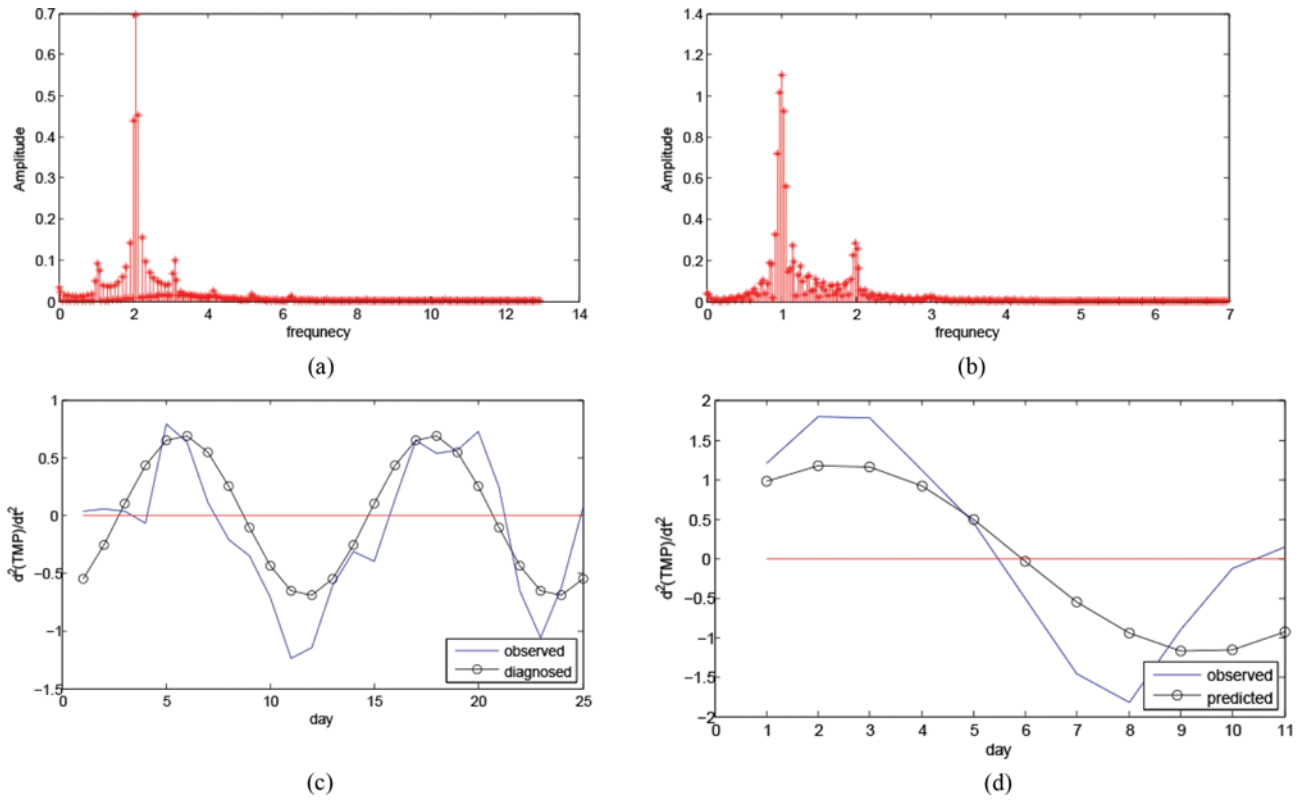

Fig. 7. Period2 results of the FFT for (a) slow fouling and (b) TMP jump, and the periodic pattern using the second derivative of TMP for (c) slow fouling and (d) TMP jump.

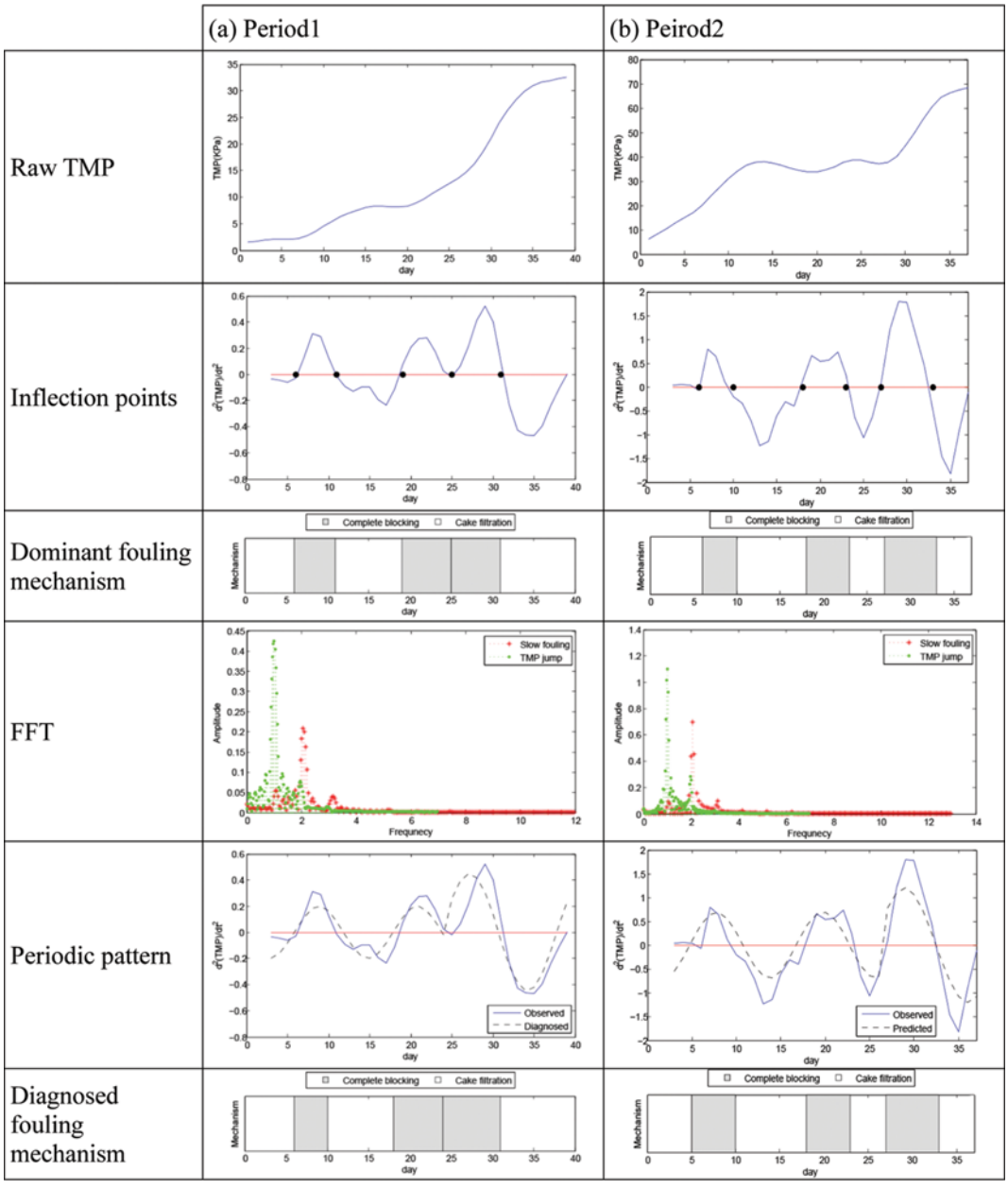

Fig. 8. The summarized results of the proposed method for diagnosing the dominant fouling mechanism: (a) Period1 and (b) period2.

dominant mechanism computed from the periodic pattern had an identical result, indicating that the periodic pattern properly identifies the dominant fouling mechanism. It can be expected that the proposed method of determining the dominant fouling mechanism contributes to the diagnosis of variations in the fouling mechanism and operation conditions of the MBR process. Moreover, the proposed method can contribute to select appropriate membrane cleaning control strategies based on the dominant fouling mechanism. Physical cleaning, such as coarse bubble aeration and relaxation, is proper when reversible fouling is dominant, *i.e.*, cake layer formation fouling, while chemical cleaning, which removes tenacious materials inside the membrane, is conducted by adding chemicals inside the membrane when irreversible fouling for pore blocking fouling is dominant [17]. Therefore, the suggested diagnosis method can be used to interpret the variation of fouling mechanism, which can decide which control action is the proper cleaning control action.

4. Results of the Fouling Diagnosis in a Lab Scale MBR Experiment

Fig. 9 shows the application results of the proposed method in the lab scale MBR experiment. Nine inflection points and ten mechanism changing intervals were computed from the second derivative of TMP, according to the tendency of the second derivative of TMP obtained in the section of '1. Determination of the dominant fouling mechanism' cake filtration was dominant when the second derivative was concave upward. On the other hand, cake filtration was the dominant mechanism when the second derivative was concave downward. These results coincide with the domi-

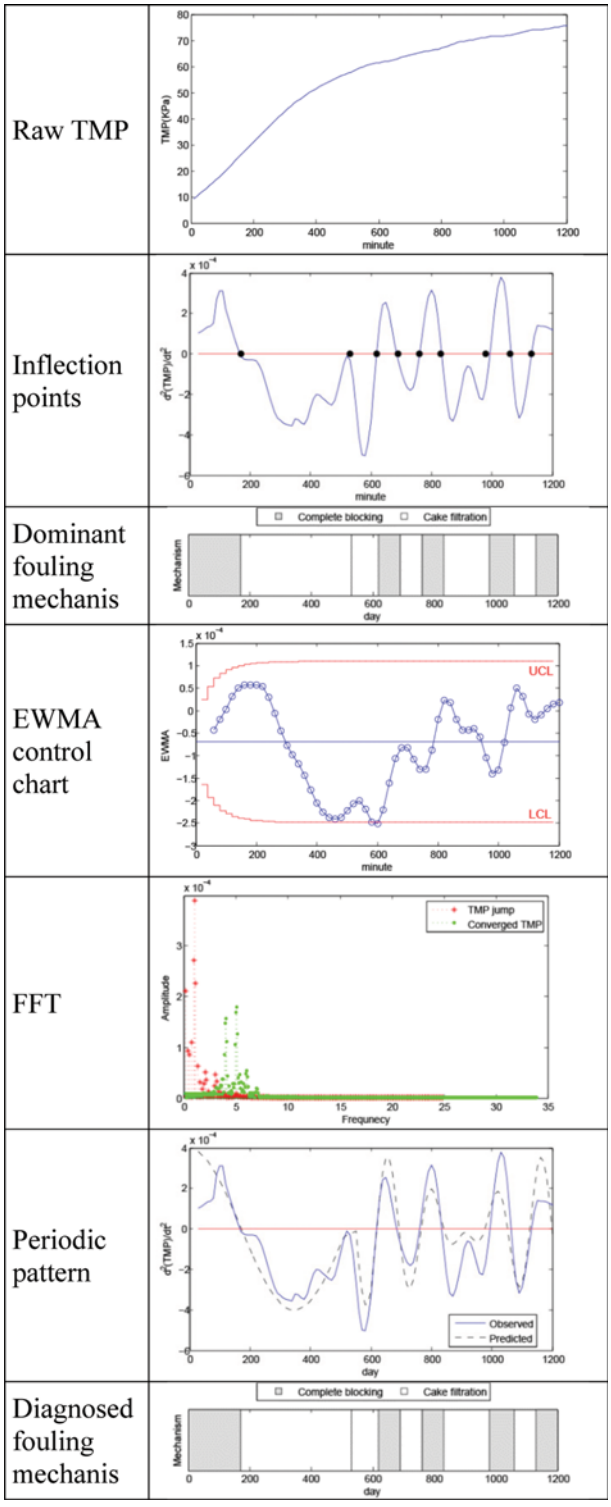

Fig. 9. Validation of the proposed method using a lab-scale MBR process.

nant fouling mechanisms that were determined by comparing the RMSE values of the four different fouling mechanisms at each interval.

Then, EWMA was applied to separate the fouling stages. The EWMA values started to decrease from 530 minutes and were below the LCL at 600 minutes. This result indicates that the second derivative of TMP had abnormal conditions at 530 minutes. The raw TMP data rapidly increased until 530 minutes, and was converted to a diminished increasing tendency after 530 minutes. Therefore, this result indicates that the fouling stage was changed at the fiducial time, which was 530 minutes. The slow TMP rise stage was not observed in the lab-scale MBR experiment. The absence of that stage can be explained by a flux condition set point. The pilot scale MBR process was operated under a constant flux of 17.0139 $L/M^2/h$. On the other hand, the lab-scale MBR experiment was operated under a constant flux of 38.5714 $L/M^2/h$. Under high constant flux conditions, foulants moved to and accumulated onto the membrane surface more rapidly than with diffusion and cross-flow shear forces, which are the inhibition mechanisms of foulant accumulation. Therefore, this phenomenon increased the resistance of water transport through the membrane, reduced the slow TMP rise stage time, and accounted for the early appearance of the TMP jump stage [41,42]. This result implies that the slow TMP rise stage did not appear and the fouling mechanism was changed from the TMP jump to converged TMP after 530 minutes.

Once the FFT method was applied to the filtered second derivative TMP of the TMP jump and converged TMP stages, the amplitude and frequency of the periodic pattern for diagnosing the dominant fouling mechanism at the TMP jump stage were 0.0004 and 2, respectively, while those at the converged TMP stage were 0.0017, 4 and 0.0019, 5, respectively. The dominant fouling mechanisms diagnosed by the periodic pattern were consistent with the observed dominant fouling mechanisms that were calculated by the four fouling mechanism fitting with the observed raw TMP.

CONCLUSIONS

A trigonometric periodic pattern for diagnosing the dominant fouling mechanism has been proposed by using differential calculus, EWMA, and FFT to investigate the complex fouling mechanism variation in the MBR process. The periodic pattern took into consideration the curvature tendency of the characteristics of the fouling mechanisms, such as downward and upward concavity, according to the increasing tendency. The periodic pattern had smooth signal information, because the high frequency noise of the real MBR process was eliminated by the filter. The predicted fouling mechanism was consistent with the real MBR process fouling mechanism determined by RMSE. Therefore, the periodic pattern had considerable ability to diagnose the dominant fouling mechanism according to time. Furthermore, the suggested periodic pattern showed adaptability in the pilot-scale MBR process and the lab-scale MBR experiment. Therefore, the periodic pattern can be used to help to understand and diagnose the operation conditions for evaluating membrane fouling of the MBR process. By evaluating membrane fouling, MBR can also operate in an environmentally friendly and economical manner by using the adaptive membrane cleaning method of the evaluated MBR operating conditions.

ACKNOWLEDGEMENT

This work was supported by the National Research Foundation

of Korea (NRF) grant funded by the Korean government (MSIP) (No. 2015R1A2A2A11001120).

REFERENCES

1. F. Xie, J. Liu, J. Wang and W. Chen, *Korean J. Chem. Eng.*, **33**, 2169 (2016).
2. H. Adib, S. Hassanajili, M. R. Sheikhi-Kouhsar, A. Salahi and T. Mohammadi, *Korean J. Chem. Eng.*, **32**, 159 (2015).
3. M. S. Muhamad, M. R. Salim and W. J. Lau, *Korean J. Chem. Eng.*, **32**, 2319 (2015).
4. A. Abdelrasoul, H. Doan, A. Lohi and C. H. Cheng, *Korean J. Chem. Eng.*, **33**, 1014 (2016).
5. A. Drews, *J. Membr. Sci.*, **363**, 1 (2010).
6. G. Bolton, D. LaCasse and R. Kuriyel, *J. Membr. Sci.*, **277**, 75 (2006).
7. Z. Wang, J. Ma, C. Y. Tang, K. Kimura, Q. Wang and X. Han, *J. Membr. Sci.*, **468**, 276 (2014).
8. X. Shi, G. Tal, N. P. Hankins and V. Gitis, *J. Water Process Eng.*, **1**, 121 (2014).
9. H. Nourbakhsh, Z. Emam-Djomeh, H. Mirsaeedghazi, M. Omid and S. Moieni, *Int. J. Food Sci. Technol.*, **49**, 58 (2014).
10. S. Mondal and S. De, *J. Membr. Sci.*, **344**, 6 (2009).
11. A. E. Contreras, A. Kim and Q. Li, *J. Membr. Sci.*, **327**, 87 (2009).
12. M. Yao, B. Ladewig and K. Zhang, *Desalination*, **278**, 126 (2011).
13. J. W. Polderman and J. C. Willems, *Introduction to the mathematical theory of systems and control*, Springer, New York (1998).
14. D. A. Serel and H. Moskowitz, *Eur. J. Oper. Res.*, **184**, 157 (2008).
15. Y. Liu, L. Guo, Q. Wang, G. An, M. Guo and H. Lian, *Mech. Syst. Signal Proc.*, **24**, 2961 (2010).
16. T. Chai and R. R. Draxler, *Geosci. Model Dev.*, **7**, 1247 (2014).
17. S. Judd, *The MBR book: principles and applications of membrane bioreactors for water and wastewater treatment*, Elsevier, Amsterdam (2010).
18. M. Y. Chen and B. T. Chen, *Appl. Soft. Comput.*, **14**, 156 (2014).
19. M. J. Kim, G. Y. Yoo and C. K. Yoo, *Asia Pac. J. Chem. Eng.*, **6**, 423 (2011).
20. M. Hlavacek, F. Bouchet, *J. Membr. Sci.*, **82**, 285 (1993).
21. E. Iritani, *Dry. Technol.*, **31**, 146 (2013).
22. J. Stewart, *Calculus early transcendentals*, CT: Brooks/Cole Cengage Learning, Stamford (2010).
23. E. Carey, *Undergrad. J. Math. Model.: One+ Two*, **1**, 2 (2009).
24. S. H. Yoon, *Membrane bioreactor processes: Principles and applications*, CRC Press, Florida (2016).
25. P. K. Gkotsis, D. C. Banti, E. N. Peleka, A. I. Zouboulis and P. E. Samaras, *Process.*, **2**, 759 (2014).
26. J. Zhang, H. C. Chua, J. Zhou and A. G. Fane, *J. Membr. Sci.*, **284**, 54 (2006).
27. B. K. Hwang, C. H. Lee, I. S. Chang, A. Drews and R. Field, *J. Membr. Sci.*, **419**, 33 (2012).
28. S. Chang, A. G. Fane and S. Vigneswaran, *AIChE J.*, **48**, 2203 (2002).
29. C. C. Ho and A. L. Zydney, *J. Membr. Sci.*, **209**, 363 (2002).
30. D. A. Serel and H. Moskowitz, *Eur. J. Oper. Res.*, **184**, 157 (2008).
31. L. A. Jones, C. W. Champ and S. E. Rigdon, *Technometrics*, **43**, 156 (2012).
32. P. Čisar and S. M. Čisar, *Acta Polytech. Hung.*, **8**, 73 (2011).
33. D. F. Elliott, *Handbook of digital signal processing: engineering applications*, Academic Press, New York (2013).
34. C. Leys, C. Ley, O. Klein, P. Bernard and L. Licata, *J. Exp. Soc. Psychol.*, **49**, 764 (2013).
35. N. Abbas, M. Riaz and R. J. Does, *Qual. Reliab. Eng. Int.*, **27**, 821 (2011).
36. D. C. Montgomery, *Introduction to statistical quality control*, John Wiley & Sons, New York (2007).
37. D. Noskievicová, *Int. J. Eng. Bus. Manage.*, **5**, 13 (2013).
38. G. Tzimiropoulos, V. Argyriou, S. Zafeiriou and T. Stathaki, *IEEE Trans. Pattern Anal. Mach.*, **32**, 1899 (2010).
39. Y. T. Sha, C. C. Bao, M. S. Jia and X. Liu, *IEEE Intl. Conf. Acoustics Speech and Signal Processing*, 381 (2010).
40. M. J. Kim, Ph.D. Thesis, Kyung Hee Univ., Korea (2016).
41. D. J. Miller, S. Kasemset, D. R. Paul and B. D. Freeman, *J. Membr. Sci.*, **454**, 505 (2014).
42. H. D. Park, I. S. Chang and K. J. Lee, *Principles of Membrane Bioreactors for Wastewater Treatment*, CRC Press, Florida (2015).